Research Paper
Computational Methods for Differential Equations
http://cmde.tabrizu.ac.ir
Vol. *, No. *, *, pp. 1-19
DOI:10.22034/cmde.2025.66344.3090

A Collocation Approach Using Cubic Unified Extended Trigonometric Tension B-Splines for Solving the Time-Fractional Telegraph Equation

Mohammad Tamsir[1], Neeraj Dhiman[2], Deependra Nigam[2,3,*], Anand Chauhan[2], and Waleed Adel[4,5,*]

[1]Department of Mathematics, College of Science, Jazan University, P.O. Box 114, Jazan 45142, Saudi Arabia.

[2]Department of Mathematics, Graphic Era Deemed to be University, Dehradun-248002, India.

[3]Department of Mathematics, D.A.V. (P.G.) College, Dehradun -248002, India.

[4]Laboratoire Interdisciplinaire de L'Universite' Francaise D'Egypte (UFEID Lab), Universite' Francaise D'Egypte, Cairo 11837, Egypt.

[5]Department of Mathematics and Engineering Physics, Faculty of Engineering, Mansoura University, Egypt.

Abstract

This paper presents a numerical collocation method based on Cubic Unified Extended Trigonometric Tension B-Spline (CUETTB-spline) functions for solving the Time Fractional Telegraph (TFT) equation. The time-fractional derivative in the TFT equation is discretized using Caputo's definition, followed by the construction of a CUETTB-spline based collocation method to approximate the solution. The precision and efficiency of the proposed method are demonstrated through three numerical examples, where the results are compared against existing methods for the error norms L_2, L_∞, and the RMS. The findings reveal that the proposed method achieves higher accuracy than previously reported approaches. Furthermore, a detailed stability analysis confirms that the method is unconditionally stable, while the rate of convergence (ROC) analysis establishes an order of $O(h^2, \tau^{2-\alpha})$. The results validate the robustness and effectiveness of the proposed method for solving the time-fractional telegraph equation.

Keywords. Caputo TFT equation; CUETTB-spline functions; Collocation technique; Stability analysis; Convergence.

2010 Mathematics Subject Classification. 65L05, 34K06, 34K28.

1. Introduction

Fractional calculus is implemented efficiently to show various physical phenomena in engineering sciences [18, 25]. Numerous applications are reported that are usually conveyed by fractional partial differential equations (PDEs). For example, Sabermahani [31] proposed a new set of fractional functions based on the Lagrange polynomials to approximate a class of fractional differential equations (FDEs). The authors of [32] presented a numerical method based on two-dimensional Müntz–Legendre hybrid functions to solve FPDEs. Rahimkhani et al. [26] used Bernoulli wavelets and the least squares support vector regression to develop a new hybrid method to approximate systems of FDEs. In addition, several phenomena such as propagation of analog and digital signals across media [17], random walk [6], and neutrons diffusive transport in nuclear reactors [36] are portrayed by a class of hyperbolic PDEs, so-called fractional telegraph equations [10]. This model is a hyperbolic type, which means the speed of the wave and the propagation are finite. It requires two initial conditions for the uniqueness, even if the order of the model is any number. The suspension flows are best modeled by the time fractional telegraph equation. The rise of such an important model gives its importance, and researchers have been investigating the possible solution for such an equation. However, it is noted that few analytical and numerical methods exist in the literature to solve the TFT equation. For example, the natural transform decomposition method is applied by the authors of [1, 9] to approximate TFT equations, while the authors of [8] applied the homotopy analysis method to approximate it. Momani [20]

Received: 11 March 2025 ; Accepted: 28 July 2025.
∗ Corresponding authors. Email: yashdeependra.ekta@gmail.com, waleed.ouf@ufe.edu.eg.

used the ADM to approximate the space-time fractional telegraph (STFT) equations. Wei et al. [37] developed a fully discrete local discontinuous Galerkin finite element method (GFEM), while Tasbozan and Esen [34] applied the Galerkin method based on Quadratic B-Spline (QBS) functions. The authors of [4, 28, 29, 41] employed collocation methods based on the cubic trigonometric B-spline (CTBS) function, Sinc-Legendre, Sinc-Chebyshev polynomials, and redefined extended uniform cubic B-spline (CBS) functions, respectively, to approximate it numerically. Tasbozan and Esen [35] applied the FEM based on CBS functions. Mishra et al. [7, 21] used a collocation method based on Legendre functions and a meshless method by amalgamation of Chebyshev polynomials and cubic RBF to approximate STFT equations. Hosseini et al. [11] implemented a technique by coupling radial basis functions with FDM for the numerical approximation of the TFT equation, while the authors of [12, 40] presented Legendre wavelet methods. Hariharan et al. [13] introduced a capable operational matrix approach based on Haar wavelets to approximate space-and-time-fractional telegraph equations. In [22, 30], the authors proposed operational matrix approaches using block pulse functions with a combination of Legendre polynomials and Fibonacci wavelets to approximate TFT equations, respectively.

Additionally, Abdollahy et al. [2] proposed the Haar wavelets approach to investigate the time fractional Riesz space telegraph equation. For the stable density, Fourier transformation solutions, for any α, are investigated by Orsingher and Beghin [23], while Orsingher and Zhao [24] investigated the Fourier transform of the space-fractional telegraph equation's elementary solution. Hashmi et al. [14] suggested a DQM based on CBS functions for the TFT equation. An amalgamation of geometric procedure and method of line is presented by Hashemi and Baleanu [15], while Asgari et al. [3] proposed a new technique using Bernstein polynomials. In [16, 19], the authors employed FDM with generalized fractional derivative terms and a Neural Network method to approximate the TFT equation, respectively. Wang et al. [39] introduced a piecewise approach with the reproducing kernel space for a class of aforesaid equation. For more information, the reader may refer to [4, 7] and references therein.

Since B-spline functions have abundant striking properties and are the vector space's basis generated by the splines with the least support for an assured degree of smoothness and subdivisions of the domain. The present spline functions, such as B-splines, hyperbolic and usual polynomial B-spline functions, etc., are all remarkable situations of unified and extended splines (UE-splines). In recent times, [38] introduced hyperbolic, polynomial, and trigonometric UE-splines. The authors of [5] reported a scheme based on trigonometric tension B-spline functions.

This work is presented to adapt the CUETTB-spline collocation method for solving the fractional order telegraph-type equations. Since most real-world physical problems can be excellently demonstrated with the fractional telegraph equation, the approximation approaches, and their stability and consistency are essential. The proposed CUETTB-spline collocation method offers several important advantages that enhance its practical applicability and robustness over other compared to other methods, such as the spectral and pseudo-spectral methods. The method is based on basis functions with local support and tunable tension parameters, which allow for greater flexibility in capturing sharp gradients and localized features in the solution, scenarios where global spectral methods often struggle. Additionally, the structure of the collocation scheme leads to sparse linear systems, resulting in lower computational complexity and memory requirements compared to the dense matrices typical of spectral approaches. This advantage is demonstrated in the comparative CPU time performance across multiple test cases. Moreover, the method is unconditionally stable, as confirmed through von Neumann stability analysis, and achieves second-order convergence in space and fractional-order convergence in time. The use of CUETTB-spline functions also enables straightforward implementation on non-uniform meshes and complex domains, unlike spectral methods, which often require transformations into orthogonal function spaces. Finally, the numerical results presented in this study, including very low error norms and strong agreement with exact solutions, validate the accuracy, efficiency, and reliability of the proposed method as a competitive alternative for solving time-fractional telegraph equations.

Motivated by the above points, we aim to utilize the CUETTB-spline approach to approximate the TFT equation. The novelty of our paper lies within the following points:

(1) We introduce a novel collocation scheme based on CUETTB-spline functions to approximate the solutions for the TFT equation.
(2) The proposed method innovatively integrates Caputo's definition to discretize the time-fractional derivative, enabling the accurate handling of fractional-order problems.

(3) A detailed stability analysis is presented to confirm that the proposed method is unconditionally stable.
(4) The efficiency and accuracy of the method are demonstrated through three diverse numerical examples, showcasing its versatility in solving TFT equations.
(5) The method's results highlight its potential for practical applications in fields requiring accurate solutions to fractional-order telegraph equations.

The rest of the article is organized as follows. Section 2 illustrates the formulation of the model, followed by section 3, which highlights the CUETTB-spline basis functions and the collocation technique. Section 4 gives a full discretization of the problem, while section 5 analyzes the stability of the discretized system of the TFT equation. The results obtained and discussion are presented in section 6. Finally, section 7 completes the study.

2. Problem Formulation

This section illustrates the main problem formulation of the model under study. The main goal of this work is to demonstrate an efficient, accurate, and stable approach for the following TFT equation [4, 21, 41]. The main problem is of the following form:

$$\frac{\partial^{\alpha} v}{\partial \tau^{\alpha}}+\lambda_1 \frac{\partial^{\alpha-1} v}{\partial \tau^{\alpha-1}}+\lambda_2 v=\lambda_3 \frac{\partial^2 v}{\partial \xi^2}+f(\xi, \tau), \ 1<\alpha<2, \tag{2.1}$$

associated with the following initial and boundary conditions

$$v(\xi, 0)=\phi_1(\xi), \ v_\tau(\xi, 0)=\phi_2(\xi), \ 0 \leq \xi \leq 1, \tag{2.2}$$

$$v(0, \tau)=\psi_1(\tau), \ v(1, \tau)=\psi_2(\tau), \ 0 \leq \tau \leq 1, \tag{2.3}$$

where λ_1, λ_2, λ_3, α, $\phi_1(\xi)$, $\phi_2(\xi)$, $\psi_1(\tau)$, and $\psi_2(\tau)$ are given constants and functions. The fractional derivatives considered in the problem are in the Caputo sense and are given by [11]

$$\frac{\partial^{\alpha} v}{\partial \tau^{\alpha}}=\begin{cases}\frac{1}{\overline{j-\alpha}} \int_0^{\tau} \frac{\partial^j v}{\partial s^j}(\tau-s)^{j-\alpha-1} d s, & \text{if } j-1<\alpha<j \\ \frac{\partial^j v}{\partial s^j}, & \text{if } \alpha=j\end{cases} \tag{2.4}$$

3. CUETTB-spline basis functions

In this section, the authors illustrate the cubic unified extended trigonometric tension B-spline basis functions that are used for the proposed collocation technique. First, the domain $\xi \in[0, 1]$ is partitioned uniformly into a mesh of length $h=\frac{1}{M}$, by the knots $\xi_i=ih$ $i=0,1,\ldots,M$, so that we possess $0=\xi_0<\xi_1<\xi_2<\ldots<\xi_M=1$. Now, in the span of $\{\cos\varsigma\xi,\ \sin\varsigma\xi,\ 1,\ \xi,\ \xi^2,\ldots\xi^l,\ldots\}$where l is a positive integer, we define the UE-spline functions of second order $(r=2)$ as [38]

$$\hat{T}_{i,2}(\xi)=\frac{1}{\sin(\varsigma h)}\begin{cases}\sin(\varsigma(\xi-\xi_{i-2})), & [\xi_{i-2}, \xi_{i-1}), \\ \sin(\varsigma(\xi_i-\xi)), & [\xi_{i-1}, \xi_i), \\ 0, & \text{Otherwise},\end{cases} \tag{3.1}$$

Here $\varsigma=\sqrt{\bar{\varsigma}_j}$ and $\bar{\varsigma}_j \in \mathrm{R}$ are the frequency sequence and the tension parameter, respectively. The tension parameter ς bears a value as a zero, real nonzero, or pure imaginary number based on $\bar{\varsigma}_j=0$, $\bar{\varsigma}_j>0$, $\bar{\varsigma}_j<0$. To ensure the non-negativity, we proceed with $\bar{\varsigma}_j \leq \min_{k=j,j+1}(\pi/(\xi_{k+1}-\xi_k))^2$. The recurrence formula for $r \geq 3$ is given as:

$$\hat{T}_{i,r}(x)=\int_{-\infty}^{\xi}\left(\delta_{i,r-1}\hat{T}_{i,r-1}(s)-\delta_{i+1,r-1}\hat{T}_{i+1,r-1}(s)\right) ds, \tag{3.2}$$

where $\delta_{i,r}=\left(\int_{-\infty}^{\infty}\hat{T}_{i,r}(s)ds\right)^{-1}, i=0,\pm1,\ldots$. Additionally, $\hat{T}_{i,m}(\xi)=0$, then we take

$$\int_{-\infty}^{\xi}\delta_{i,r}\hat{T}_{i,r}(s)ds=\begin{cases}1, & \xi \geq \xi_{i+r-2}, \\ 0, & \xi<\xi_{i+r-2}.\end{cases}$$

If $0 < \varsigma \leq \frac{\pi}{h}$, the aforementioned spline functions are trigonometric. Using (3.2) for $r = 3$ with $0 < \bar{\varsigma}_j \leq \min_{k=j,j+1} (\pi/(\xi_{k+1} - \xi_k))^2$, the quadratic unified extended trigonometric tension B-spline functions of order 3 can be obtained as follows:

$$\hat{T}_{i,3}(\xi) = \frac{1}{1-\cos(\varsigma h)} \begin{cases} 1 - \cos(\varsigma(\xi - \xi_{i-2})), & [\xi_{i-2}, \xi_{i-1}) \\ -1 + \cos(\varsigma(\xi_i - \xi)) - \cos(\varsigma h) + \cos(\varsigma(\xi - \xi_{i-1})), & [\xi_{i-1}, \xi_i) \\ 1 - \cos(\varsigma(\xi_{i+1} - \xi)), & [\xi_i, \xi_{i+1}) \\ 0, & else. \end{cases} \tag{3.3}$$

Now, utilizing the recursive formula (3.2) for $r = 4$ and taking $0 < \varsigma \leq \frac{\pi}{h}$, the 4^{th} order CEUTTB-spline functions can be found as [5]:

$$\hat{T}_{i,4}(\xi) = \frac{1}{\vartheta} \begin{cases} (\xi - \xi_{i-2}) - \frac{\sin(\varsigma(\xi_{i-2} - \xi)}{\eta}, & \xi \in [\xi_{i-2}, \xi_{i-1}) \\ (\xi_i - \xi) + (2\xi_{i-1} - \xi)\cos(\varsigma h) - \frac{2\sin(\varsigma(\xi_{i-1} - \xi)) + \sin(\varsigma(\xi_i - \xi))}{\eta}, & \xi \in [\xi_{i-1}, \xi_i) \\ (\xi - \xi_i) - (2\xi_{i+1} - \xi)\cos(\varsigma h) + \frac{\sin(\varsigma(\xi_i - \xi)) + 2\sin(\varsigma(\xi_{i+1} - \xi))}{\eta}, & \xi \in [\xi_i, \xi_{i+1}) \\ (\xi_{i+2} - \xi) - \frac{\sin(\varsigma(\xi_{i+2} - \xi)}{\varsigma}, & \xi \in [\xi_{i+1}, \xi_{i+2}) \\ 0, & \text{Otherwise.} \end{cases} \tag{3.4}$$

where, $\vartheta = 2h(1 - \cos(\varsigma h))$. The CUETTB-spline functions $\left\{\hat{T}_{0,4}, \hat{T}_{1,4}, ..., \hat{T}_{M,4}, \hat{T}_{M+1,4}\right\}$ form a basis over the problem domain. The CUETTB-spline functions and their derivatives values at knots are given in Table 1, where $\sigma_1 = \frac{1}{\vartheta}\left(h - \frac{\sin(\varsigma h)}{\varsigma}\right)$ $\sigma_2 = \frac{1}{\vartheta}\left(\frac{2\sin(\varsigma h)}{\varsigma} - 2h\cos(\varsigma h)\right)$, $\sigma_3 = -\frac{1-\cos(\varsigma h)}{\vartheta}$, $\sigma_4 = \frac{\varsigma \sin(\varsigma h)}{\vartheta}$, and $\sigma_5 = -\frac{2\varsigma \sin(\varsigma h)}{\vartheta}$.

TABLE 1. Values of $\hat{T}_{i,4}(\xi)$, $\hat{T}'_{i,4}(\xi)$, and $\hat{T}''_{i,4}(\xi)$ at knots ξ_i.

	ξ_{i-2}	ξ_{i-1}	ξ_i	ξ_{i+1}	ξ_{i+2}
$\hat{T}_{i,4}(\xi)$	0	σ_1	σ_2	σ_1	0
$\hat{T}'_{i,4}(\xi)$	0	σ_3	0	$-\sigma_3$	0
$\hat{T}''_{i,4}(\xi)$	0	σ_4	σ_5	σ_4	0

We define the approximated solution as

$$v(\xi, \tau^j) \cong \sum_{i=-1}^{M+1} \hat{T}_{i,4}(\xi) C_i(\tau^j), \tag{3.5}$$

where $C_i(t_j)$ are unknown time-dependent quantities. The variation of the $v(\xi, \tau_j)$ is asserted as

$$v(\xi, \tau_j) = \sum_{k=i-1}^{i+1} \hat{T}_{k,4}(\xi) C_k(\tau_j). \tag{3.6}$$

Using (3.6), we approximated v v_ξ, and $v_{\xi\xi}$ as

$$v_i^j = \sigma_1 C_{i-1}^j + \sigma_2 C_i^j + \sigma_1 C_{i+1}^j, \tag{3.7}$$

$$(v_\xi)_i^j = -\sigma_3 C_{i-1}^j + \sigma_3 C_{i+1}^j, \tag{3.8}$$

$$(v_{\xi\xi})_i^j = \sigma_4 C_{i-1}^j + \sigma_5 C_i^j + \sigma_4 C_{i+1}^j. \tag{3.9}$$

Next, we demonstrate the discretization of the main model to be solved by the proposed technique.

4. Discretization of the problem

In this section, we highlight the discretization procedure to solve the main problem. According to the considered problem (2.1), the fractional derivatives can be written as [11]

$$\frac{\partial^\alpha v}{\partial \tau^\alpha} = \begin{cases} \frac{1}{\Gamma 2-\alpha} \int_0^\tau \frac{\partial^2 v}{\partial s^2} (\tau - s)^{1-\alpha} ds, & \text{if } 1 < \alpha < 2, \\ \frac{\partial^2 v}{\partial \tau^2}, & \text{if } \alpha = 2, \end{cases}, \tag{4.1}$$

and

$$\frac{\partial^{\alpha-1} v}{\partial \tau^{\alpha-1}} = \begin{cases} \frac{1}{\Gamma 2-\alpha} \int_0^\tau \frac{\partial v}{\partial s} (\tau - s)^{1-\alpha} ds, & \text{if } 1 < \alpha < 2, \\ \frac{\partial^2 v}{\partial \tau^2}, & \text{if } \alpha = 2. \end{cases} \tag{4.2}$$

The discretization of $\frac{\partial^\alpha v}{\partial \tau^\alpha}$ and $\frac{\partial^{\alpha-1} v}{\partial \tau^{\alpha-1}}$ for $1 < \alpha < 2$ at $\tau = \tau^{j+1}$ is given as [11]

$$\frac{\partial^\alpha v_i^{j+1}}{\partial \tau^\alpha} = a_0 \sum_{k=0}^{j} P_k \left(v_i^{j-k+1} - 2v_i^{j-k} + v_i^{j-k-1} \right) + r_1^{j+1}, j = 0, 1, ..., N, \tag{4.3}$$

and

$$\frac{\partial^{\alpha-1} v_i^{j+1}}{\partial \tau^{\alpha-1}} = a_0 \Delta\tau \sum_{k=0}^{j} P_k \left(v_i^{j-k+1} - v_i^{j-k} \right) + r_2^{j+1}, j = 0, 1, ..., N, \tag{4.4}$$

where $a_0 = \frac{\Delta\tau^{-\alpha}}{\Gamma 3-\alpha}$, $P_k = (k+1)^{2-\alpha} - k^{2-\alpha}$, $\forall k = 0, 1, 2....j$, while r_1^{j+1} and r_2^{j+1} are truncation errors at $\tau = \tau^{j+1}$. Now, $\tau = \tau^{j+1}$, using Equations (4.3) and (4.4) for time-fractional derivatives and the Crank-Nicolson scheme for spatial derivatives, we get

$$\begin{aligned} &a_0 \sum_{k=0}^{j} P_k \left(v_i^{j-k+1} - 2v_i^{j-k} + v_i^{j-k-1} \right) + \lambda_1 a_0 \Delta\tau \sum_{k=0}^{j} P_k \left(v_i^{j-k+1} - v_i^{j-k} \right) + \lambda_2 \frac{\left(v_i^{j+1} + v_i^j \right)}{2} \\ &= \lambda_3 \frac{\left((v_{\xi\xi})_i^{j+1} + (v_{\xi\xi})_i^j \right)}{2} + \frac{\left(f_i^{j+1} + f_i^j \right)}{2}, \qquad i = 0, 1, ..., M, j = 0, 1, ..., N. \end{aligned} \tag{4.5}$$

Rearranging the terms in (4.5), we get

$$\begin{aligned} \left(a_0 + \lambda_1 a_0 \Delta\tau + \frac{\lambda_2}{2} \right) v_i^{j+1} - \frac{\lambda_3}{2} (v_{\xi\xi})_i^{j+1} = &\left(2a_0 + \lambda_1 a_0 \Delta\tau - \frac{\lambda_2}{2} \right) v_i^j + \frac{\lambda_3}{2} (v_{\xi\xi})_i^j - a_0 v_i^{j-1} \\ &- a_0 \sum_{k=1}^{j} P_k \left(v_i^{j-k+1} - 2v_i^{j-k} + v_i^{j-k-1} \right) \\ &- \lambda_1 a_0 \Delta\tau \sum_{k=1}^{j} P_k \left(v_i^{j-k+1} - v_i^{j-k} \right) + \frac{\left(f_i^{j+1} + f_i^j \right)}{2}, \\ &i = 0, 1, ..., M, j = 0, 1, ..., N. \end{aligned} \tag{4.6}$$

For $j = 0$, using the initial condition $v_\tau(\xi, 0) = \phi_2(\xi)$, i.e.

$$\frac{v_i^1 - v_i^{-1}}{2\Delta\tau} = \phi_2(\xi_i) \Rightarrow v_i^{-1} = v_i^1 - 2\Delta\tau\phi_2(\xi_i),$$

we obtain the following

$$\left(2a_0+\lambda_1 a_0\Delta\tau+\frac{\lambda_2}{2}\right)v_i^1-\frac{\lambda_3}{2}\left(v_{\xi\xi}\right)_i^1=\left(2a_0+\lambda_1 a_0\Delta\tau-\frac{\lambda_2}{2}\right)v_i^0+\frac{\lambda_3}{2}\left(v_{\xi\xi}\right)_i^0+2a_0\Delta\tau\phi_2\left(\xi_i\right)+\frac{\left(f_i^{j+1}+f_i^j\right)}{2},\qquad i=0,1,...,M. \tag{4.7}$$

Let $2a_0+\lambda_1 a_0\Delta\tau+\frac{\lambda_2}{2}=\hat{A}$ and $2a_0+\lambda_1 a_0\Delta\tau-\frac{\lambda_2}{2}=\hat{B}$, then the above equation becomes

$$\hat{A}v_i^1-\frac{\lambda_3}{2}\left(v_{\xi\xi}\right)_i^1=\hat{B}v_i^0+\frac{\lambda_3}{2}\left(v_{\xi\xi}\right)_i^0+\frac{\left(f_i^1+f_i^0\right)}{2}+2a_0\Delta\tau\phi_2\left(\xi_i\right),\ i=0,1,...,M. \tag{4.8}$$

Now, using approximated values of spatial derivatives by the CEUTTB-spline collocation technique, we get

$$\left(\hat{A}\sigma_1-\frac{\lambda_3\sigma_4}{2}\right)C_{i-1}^1+\left(\hat{A}\sigma_2-\frac{\lambda_3\sigma_5}{2}\right)C_i^1+\left(\hat{A}\sigma_1-\frac{\lambda_3\sigma_4}{2}\right)C_{i+1}^1=\left(\hat{B}\sigma_1+\frac{\lambda_3\sigma_4}{2}\right)C_{i-1}^0$$
$$+\left(\hat{B}\sigma_2+\frac{\lambda_3\sigma_5}{2}\right)C_i^0+\left(\hat{B}\sigma_1+\frac{\lambda_3\sigma_4}{2}\right)C_{i+1}^0+2a_0\Delta\tau\phi_2\left(\xi_i\right)+\frac{\left(f_i^1+f_i^0\right)}{2},\qquad i=1,2...,M-1. \tag{4.9}$$

Using $\hat{A}\sigma_1-\frac{\lambda_3\sigma_4}{2}=A^*$, $\hat{A}\sigma_2-\frac{\lambda_3\sigma_5}{2}=B^*$, $\hat{B}\sigma_1+\frac{\lambda_3\sigma_4}{2}=D^*$and $\hat{B}\sigma_2+\frac{\lambda_3\sigma_5}{2}=E^*$, the above equation, becomes

$$A^*C_{i-1}^1+B^*C_i^1+A^*C_{i+1}^1=D^*C_{i-1}^1+E^*C_i^0+D^*C_{i+1}^1+2a_0\Delta\tau\phi_2\left(\xi_i\right)+\frac{\left(f_i^1+f_i^0\right)}{2},\ i=1,2,...,M-1. \tag{4.10}$$

Equation (4.10) forms a linear system with $M+1$ equations and $M+3$ unknowns. To make it uniquely solvable, we use the boundary conditions $v\left(0,\tau\right)=\psi_1\left(\tau\right)$, and $v\left(1,\tau\right)=\psi_2\left(\tau\right)$ as

$$\sigma_1C_{-1}^j+\sigma_2C_0^j+\sigma_1C_1^j=\psi_1^j\left(\tau\right), \tag{4.11}$$

and

$$\sigma_1C_{M-1}^j+\sigma_2C_M^j+\sigma_1C_{M+1}^j=\psi_2^j\left(\tau\right). \tag{4.12}$$

Then, by solving Eqs. (4.11) and (4.12), we get

$$C_{-1}^j=-\frac{\sigma_2}{\sigma_1}C_0^j-C_1^j+\frac{1}{\sigma_1}\psi_1^j(\tau)\text{ and }C_{M+1}^j=-\frac{\sigma_2}{\sigma_1}C_M^j-C_{M-1}^j+\frac{1}{\sigma_1}\psi_2^j(\tau). \tag{4.13}$$

For $i=0$ and $i=M$, using the Eq. (4.13) in the Eq. (4.10), we get

$$\left(-\frac{\sigma_2}{\sigma_1}A^*+B^*\right)C_0^1=\left(-\frac{\sigma_2}{\sigma_1}D^*+E^*\right)C_0^0+\frac{D^*\psi_1^0}{\sigma_1}-\frac{A^*\psi_1^1}{\sigma_1}+2a_0\Delta\tau\phi_2\left(\xi_0\right)+\frac{\left(f_0^1+f_0^0\right)}{2}, \tag{4.14}$$

and

$$\left(-\frac{\sigma_2}{\sigma_1}A^*+B^*\right)C_M^1=\left(-\frac{\sigma_2}{\sigma_1}D^*+E^*\right)C_M^0+\frac{D^*\psi_2^0}{\sigma_1}-\frac{A^*\psi_2^1}{\sigma_1}+2a_0\Delta\tau\phi_2\left(\xi_M\right)+\frac{\left(f_M^1+f_M^0\right)}{2}. \tag{4.15}$$

Now, for $j=1,2,...,N$, the Eq. (4.6) can be written as

$$\left(\hat{A}-a_0\right)v_i^{j+1}-\frac{1}{2}\lambda_3\left(v_{\xi\xi}\right)_i^{j+1}=\hat{B}v_i^j+\frac{1}{2}\lambda_3\left(v_{\xi\xi}\right)_i^j-a_0v_i^{j-1}-\left(a_0+a_0\lambda_1\Delta\tau\right)\sum_{k=1}^{j}P_kv_i^{j-k+1}+$$

$$\left(2a_0+a_0\lambda_1\Delta\tau\right)\sum_{k=1}^{j}P_kv_i^{j-k}-a_0\sum_{k=1}^{j}P_kv_i^{j-k-1}-a_0P_jv_i^1+2a_0P_j\Delta\tau\phi_2\left(\xi_i\right)+\frac{\left(f_i^{j+1}+f_i^j\right)}{2}, \tag{4.16}$$

Now, using approximated values of v and $v_{\xi\xi}$ by the CEUTTB-spline collocation technique, we get

$$A^{**}C_{i-1}^{j+1}+B^{**}C_{i}^{j+1}+A^{**}C_{i+1}^{j+1}=D^{**}C_{i-1}^{j}+E^{**}C_{i}^{j}+D^{**}C_{i+1}^{j}-a_0\left(\sigma_1C_{i-1}^{j-1}+\sigma_2C_{i}^{j-1}+\sigma_1C_{i+1}^{j-1}\right)$$
$$-F^{**}\sum_{k=1}^{j}P_k\left(\sigma_1C_{i-1}^{j-k+1}+\sigma_2C_{i}^{j-k+1}+\sigma_1C_{i+1}^{j-k+1}\right)+\hat{B}\sum_{k=1}^{j}P_k\left(\sigma_1C_{i-1}^{j-k}+\sigma_2C_{i}^{j-k}+\sigma_1C_{i+1}^{j-k}\right)$$
$$-a_0\sum_{k=1}^{j-1}P_k\left(\sigma_1C_{i-1}^{j-k-1}+\sigma_2C_{i}^{j-k-1}+\sigma_1C_{i+1}^{j-k-1}\right)-a_0P_j\left(\sigma_1C_{i-1}^{1}+\sigma_2C_{i}^{1}+\sigma_1C_{i+1}^{1}\right)+2a_0P_j\Delta\tau\phi_2\left(\xi_i\right)$$
$$+\frac{\left(f_i^{j+1}+f_i^{j}\right)}{2},\qquad i=1,2,...,M-1,\quad j=1,2,...,N, \tag{4.17}$$

where $A^{**}=\left(\hat{A}-a_0\right)\sigma_1-\frac{1}{2}\lambda_3\sigma_4$, $B^{**}=\left(\hat{A}-a_0\right)\sigma_2-\frac{1}{2}\lambda_3\sigma_5$, $D^{**}=\hat{B}\sigma_1+\frac{1}{2}\lambda_3\sigma_4$, $E^{**}=\hat{B}\sigma_2+\frac{1}{2}\lambda_3\sigma_5$, and $F^{**}=a_0+a_0\lambda_1\Delta\tau$.
For $i=0$ and $i=M$, implementing the Eq. (4.13) in the above equation, we get

$$\left(-\frac{\sigma_2}{\sigma_1}A^{**}+B^{**}\right)C_0^{j+1}=\left(-\frac{\sigma_2}{\sigma_1}D^{**}+E^{**}\right)C_0^{j}+\frac{D^{**}}{\sigma_1}\psi_1^{j}-\frac{A^{**}}{\sigma_1}\psi_1^{j+1}-a_0\psi_1^{j-1}-F^{**}\sum_{k=1}^{j}P_k\psi_1^{j-k+1}$$
$$+\hat{B}\sum_{k=1}^{j}P_k\psi_1^{j+1}-a_0\sum_{k=1}^{j-1}P_k\psi_1^{j-k-1}-a_0P_j\psi_1^{1}$$
$$+2a_0P_j\Delta\tau\phi_2\left(\xi_0\right)+\frac{\left(f_0^{j+1}+f_0^{j}\right)}{2},\qquad j=1,2,...,N, \tag{4.18}$$

and

$$\left(-\frac{\sigma_2}{\sigma_1}A^{**}+B^{**}\right)C_M^{j+1}=\left(-\frac{\sigma_2}{\sigma_1}D^{**}+E^{**}\right)C_M^{j}+\frac{D^{**}}{\sigma_1}\psi_2^{j}-\frac{A^{**}}{\sigma_1}\psi_2^{j+1}-a_0\psi_2^{j-1}-F^{**}\sum_{k=1}^{j}P_k\psi_2^{j-k+1}$$
$$+\hat{B}\sum_{k=1}^{j}P_k\psi_2^{j-k}-a_0\sum_{k=1}^{j-1}P_k\psi_2^{j-k-1}-a_0P_j\psi_2^{1}$$
$$+2a_0P_j\Delta\tau\phi_2\left(\xi_M\right)+\frac{\left(f_M^{j+1}+f_M^{j}\right)}{2},\qquad j=1,2,...,N. \tag{4.19}$$

At the time τ_j $j=0,1,...,N$, the Eqs. (4.10), (4.14), and (4.15), as well as Equations (4.17)–(4.19), form a system of linear equations of $(M+1)\times(M+1)$ order. To solve these systems, we need to resolve $\left(C_0^0,C_1^0,...,C_{M-1}^0,C_M^0\right)$ from the initial condition, which provides $M+1$ equation in $N+3$ unknowns. To wipe out C_{-1}^0,C_{M+1}^0, we use the initial condition $v\left(\xi,0\right)=\phi_1\left(\xi\right)$ and its first derivative at the boundaries as follows:

$$\sigma_1C_{i-1}^0+\sigma_2C_i^0+\sigma_1C_{i+1}^0=\phi_1\left(\xi_i\right). \tag{4.20}$$

Now, for the derivative of the initial condition with respect to ξ, we get

$$-\sigma_3C_{i-1}^0+\sigma_3C_{i+1}^0=\frac{\partial\phi_1\left(\xi_i\right)}{\partial\xi}.$$

At the boundaries, we get

$$C_{-1}^0=C_1^0-\frac{1}{\sigma_3}\frac{\partial\phi_1\left(\xi_0\right)}{\partial\xi},C_{M+1}^0=C_{M-1}^0+\frac{1}{\sigma_3}\frac{\partial\phi_1\left(\xi_M\right)}{\partial\xi}. \tag{4.21}$$

For $i = 0$ and $i = M$, using Eq. (4.21) in Eq. (4.20), we get

$$\sigma_2 C_0^0 + 2\sigma_1 C_1^0 = \phi_1(\xi_0) + \frac{\sigma_1}{\sigma_3}\frac{\partial \phi_1(\xi_0)}{\partial \xi}. \tag{4.22}$$

and

$$2\sigma_1 C_{M-1}^0 + \sigma_2 C_M^0 = \phi_1(\xi_M) - \frac{\sigma_1}{\sigma_3}\frac{\partial \phi_1(\xi_M)}{\partial \xi}. \tag{4.23}$$

Eqs. (4.20), (4.22), and (4.23) form a linear system as:

$$\begin{bmatrix} \sigma_2 & 2\sigma_1 & 0 & & & & \\ \sigma_1 & \sigma_2 & \sigma_1 & & & & \\ 0 & \sigma_1 & \sigma_2 & \sigma_1 & & & \\ & \ddots & \ddots & \ddots & & & \\ & & & \sigma_1 & \sigma_2 & \sigma_1 & 0 \\ & & & & \sigma_1 & \sigma_2 & \sigma_1 \\ & & & & 0 & 2\sigma_1 & \sigma_2 \end{bmatrix} \begin{bmatrix} C_0^0 \\ C_1^0 \\ C_2^0 \\ \vdots \\ C_{M-2}^0 \\ C_{M-1}^0 \\ C_M^0 \end{bmatrix} = \begin{bmatrix} \phi_1(\xi_0) + \frac{\sigma_1}{\sigma_3}\frac{\partial \phi_1(\xi_0)}{\partial \xi} \\ \phi_1(\xi_1) \\ \phi_1(\xi_2) \\ \vdots \\ \phi_1(\xi_{M-2}) \\ \phi_1(\xi_{M-1}) \\ \phi_1(\xi_M) - \frac{\sigma_1}{\sigma_3}\frac{\partial \phi_1(\xi_M)}{\partial \xi} \end{bmatrix}. \tag{4.24}$$

In the next section, we illustrate the stability analysis of the proposed method.

5. Stability analysis

This section establishes the stability of the discretized system of the TFT equation using the von Neumann scheme [27, 34]. According to Duhamel's principle [33], it is supposed that the stability of an inhomogeneous problem is an instantaneous outcome for the stability of the equivalent homogeneous one. Therefore, it is suitable to analyze the stability of the discretized system for the TFT equation with the force function $f = 0$. With some manipulation, Eq. (4.6) can be written as

$$\begin{aligned} \left(\hat{A} - a_0\right) v_i^{j+1} - \frac{1}{2}\lambda_3 \left(v_{\xi\xi}\right)_i^{j+1} &= (a_0 + a_0\lambda_1\Delta\tau)\left(P_0 v_i^j - \sum_{k=1}^{j} P_k\left(v_i^{j-k+1} - v_i^{j-k}\right)\right) \\ &\quad - a_0\left(-P_0\left(v_i^j - v_i^{j-1}\right) - \sum_{k=1}^{j} P_k\left(v_i^{j-k} - v_i^{j-k-1}\right)\right), \end{aligned} \tag{5.1}$$

which can be written as

$$\begin{aligned} \left(\hat{A} - a_0\right) v_i^{j+1} - \frac{1}{2}\lambda_3 \left(v_{\xi\xi}\right)_i^{j+1} &= (a_0 + a_0\lambda_1\Delta\tau)\left(P_0 v_i^j - \sum_{k=0}^{j-1} P_{k+1} v_i^{j-k} + \sum_{k=1}^{j} P_k v_i^{j-k}\right) \\ &\quad - \left(-P_0\left(v_i^j - v_i^{j-1}\right) - \sum_{k=0}^{j-1} P_{k+1} v_i^{j-k-1} + \sum_{k=1}^{j} P_k v_i^{j-k-1}\right), \\ \Rightarrow \quad \left(\hat{A} - a_0\right) v_i^{j+1} - \frac{1}{2}\lambda_3 \left(v_{\xi\xi}\right)_i^{j+1} &= (a_0 + a_0\lambda_1\Delta\tau)\left((1 - P_1) v_i^j + \sum_{k=1}^{j-1}\left(P_k - P_{k+1}\right) v_i^{j-k} + P_j v^0\right) \\ &\quad - a_0\left((1 - P_1) v_i^{j-1} + \sum_{k=1}^{j-1}\left(P_k - P_{k+1}\right) v_i^{j-k-1} + P_j v_i^{-1}\right) + a_0 v_i^j. \end{aligned} \tag{5.2}$$

Eq. (5.2) can be written as

$$\left(\hat{A}-a_0\right)v_i^{j+1}-\frac{1}{2}\lambda_3\left(v_{\xi\xi}\right)_i^{j+1}=\left(a_0+a_0\lambda_1\Delta\tau\right)\left(\left(1-P_1\right)v_i^j+\sum_{k=1}^{j-1}\left(P_k-P_{k+1}\right)v_i^{j-k}+P_jv^0\right)$$
$$-a_0\left(\left(1-P_1\right)v_i^{j-1}+\sum_{k=1}^{j-1}\left(P_k-P_{k+1}\right)v_i^{j-k-1}+P_jv_i^{-1}-2\Delta\tau P_j\phi_2\left(\xi_i\right)\right)+a_0v_i^j. \tag{5.3}$$

Next, without loss of generality and for convenience, we suppose that $\phi_2=0$. Using approximated values of v and $v_{\xi\xi}$ by the CEUTTB-spline collocation technique, we get

$$\left(\left(\hat{A}-a_0\right)\sigma_1-\frac{1}{2}\lambda_3\sigma_4\right)C_{i-1}^{j+1}+\left(\left(\hat{A}-a_0\right)\sigma_2-\frac{1}{2}\lambda_3\sigma_5\right)C_i^{j+1}+\left(\left(\hat{A}-a_0\right)\sigma_1-\frac{1}{2}\lambda_3\sigma_4\right)C_{i+1}^{j+1}$$
$$=\left(a_0+a_0\lambda_1\Delta\tau\right)\Bigg[\left(1-P_1\right)\left(\sigma_1C_{i-1}^j+\sigma_2C_i^j+\sigma_1C_{i+1}^j\right)+\sum_{k=1}^{j-1}\left(P_k-P_{k+1}\right)\left(\sigma_1C_{i-1}^{j-k}+\sigma_2C_i^{j-k}+\sigma_1C_{i+1}^{j-k}\right)$$
$$+P_j\left(\sigma_1C_{i-1}^0+\sigma_2C_i^0+\sigma_1C_{i+1}^0\right)\Bigg]-a_0\Bigg[\left(1-P_1\right)\left(\sigma_1C_{i-1}^{j-1}+\sigma_2C_i^{j-1}+\sigma_1C_{i+1}^{j-1}\right)$$
$$+\sum_{k=1}^{j-1}\left(P_k-P_{k+1}\right)\left(\sigma_1C_{i-1}^{j-k-1}+\sigma_2C_i^{j-k-1}+\sigma_1C_{i+1}^{j-k-1}\right)+P_j\left(\sigma_1C_{i-1}^1+\sigma_2C_i^1+\sigma_1C_{i+1}^1\right)\Bigg]$$
$$+a_0\left(\sigma_1C_{i-1}^j+\sigma_2C_i^j+\sigma_1C_{i+1}^j\right). \tag{5.4}$$

Now, we define the growth factor of a typical Fourier mode as $C_i^j=\delta^je^{ki\mu h}$ where $k=\sqrt{-1}$ and δ is a factor dependent on time. Using in the Eq. (5.4), we get

$$\left(2A^{**}\cos(\mu h)+B^{**}\right)\delta^{j+1}=F^{**}\Bigg\{\left(1-P_1\right)\delta^j\left(2\sigma_1\cos(\mu h)+\sigma_2\right)$$
$$+\sum_{k=1}^{j-1}\left(P_k-P_{k+1}\right)\delta^{j-k}\left(2\sigma_1\cos(\mu h)+\sigma_2\right)+P_j\delta^0\left(2\sigma_1\cos(\mu h)+\sigma_2\right)\Bigg\}$$
$$-a_0\Bigg\{\left(1-P_1\right)\delta^{j-1}\left(2\sigma_1\cos(\mu h)+\sigma_2\right)$$
$$+\sum_{k=1}^{j-1}\left(P_k-P_{k+1}\right)\delta^{j-k-1}\left(2\sigma_1\cos(\mu h)+\sigma_2\right)+P_j\delta^{-1}\left(2\sigma_1\cos(\mu h)+\sigma_2\right)\Bigg\}$$
$$+a_0\left(2\sigma_1\cos(\mu h)+\sigma_2\right)\delta^j \tag{5.5}$$

where, $A^{**}=\left(\hat{A}-a_0\right)\sigma_1-\frac{1}{2}\lambda_3\sigma_4$, $B^{**}=\left(\hat{A}-a_0\right)\sigma_2-\frac{1}{2}\lambda_3\sigma_5$, and $F^{**}=a_0+a_0\lambda_1\Delta\tau$. Hence, we get the following

$$\left(2A^{**}\cos(\mu h)+B^{**}\right)\delta^{j+1}=F^{**}\left\{\left(1-P_1\right)\delta^j+\sum_{k=1}^{j-1}\left(P_k-P_{k+1}\right)\delta^{j-k}+P_j\delta^0\right\}\left(2\sigma_1\cos(\mu h)+\sigma_2\right)$$
$$-a_0\left\{\left(1-P_1\right)\delta^{j-1}+\sum_{k=1}^{j-1}\left(P_k-P_{k+1}\right)\delta^{j-k-1}+P_j\delta^1\right\}\left(2\sigma_1\cos(\mu h)+\sigma_2\right) \tag{5.6}$$
$$+a_0\left(2\sigma_1\cos(\mu h)+\sigma_2\right)\delta^j.$$

Now, we define

$$\delta^j_{\max} = \max_{0\le i\le j} \left|\delta^i\right|. \tag{5.7}$$

then by using (5.7) in (5.6), we get

$$\begin{aligned}(2A^{**}\cos(\mu h) + B^{**})\,\delta^{j+1} &= \left[F^{**}\left((1-P_1) + \sum_{k=1}^{j-1}(P_k - P_{k+1}) + P_j\right)\delta^j_{\max}\right.\\ &\quad \left. - a_0\left\{(1-P_1) + \sum_{k=1}^{j-1}(P_k - P_{k+1}) + P_j\right\}\delta^j_{\max} + a_0\delta^j_{\max}\right](2\sigma_1\cos(\mu h) + \sigma_2)\\ &\Rightarrow (2A^{**}\cos(\mu h) + B^{**})\,\delta^{j+1} = (F^{**}P_0 - a_0P_0 + a_0)\,\delta^j_{\max}\,(2\sigma_1\cos(\mu h) + \sigma_2)\\ &\Rightarrow \delta^{j+1} = \frac{(a_0 + a_0\lambda_1\Delta\tau)\,(2\sigma_1\cos(\mu h) + \sigma_2)}{2A^{**}\cos(\mu h) + B^{**}}\,\delta^j_{\max}. \end{aligned}\tag{5.8}$$

Since

$$\begin{aligned}&2A^{**}\cos(\mu h) + B^{**} = ((2a_0 + 2a_0\lambda_1\Delta\tau)\,\sigma_1 - \lambda_3\sigma_4)\cos(\mu h) + (a_0 + a_0\lambda_1\Delta\tau)\,\sigma_2 - \frac{1}{2}\lambda_3\sigma_5,\\ &\Rightarrow 2A^{**}\cos(\mu h) + B^{**} = 2a_0\,(1+\lambda_1\Delta\tau)\,\sigma_1\cos(\mu h) - \lambda_3\sigma_4\cos(\mu h) + a_0\,(1+\lambda_1\Delta\tau)\,\sigma_2 - \frac{1}{2}\lambda_3\sigma_5,\\ &\Rightarrow 2A^{**}\cos(\mu h) + B^{**} = a_0\,(1+\lambda_1\Delta\tau)\,(2\sigma_1\cos(\mu h) + \sigma_2) - \left(\lambda_3\sigma_4\cos(\mu h) + \frac{1}{2}\lambda_3\sigma_5\right),\end{aligned}$$

Finally, by using $\sigma_5 = -2\sigma_4$, we get

$$2A^{**}\cos(\mu h) + B^{**} = a_0\,(1+\lambda_1\Delta\tau)\,(2\sigma_1\cos(\mu h) + \sigma_2) + \lambda_3\sigma_4\left(2\sin^2\left(\frac{\mu h}{2}\right)\right).$$

Substituting in the Equation (5.8), we get

$$\delta^{j+1} = \frac{(a_0 + a_0\lambda_1\Delta\tau)\,(2\sigma_1\cos(\mu h) + \sigma_2)}{a_0\,(1+\lambda_1\Delta\tau)\,(2\sigma_1\cos(\mu h) + \sigma_2) + \lambda_3\sigma_4\left(2\sin^2\left(\frac{\mu h}{2}\right)\right)}\delta^j_{\max} \Rightarrow |\delta| \le 1.$$

Hence, the discretized system of the TFT equation is unconditionally stable.

6. Computational Results

In this section, we illustrate the performance of our proposed technique by testing for three examples. The following error norms are used for numerical analysis:

$$L_2 = \sqrt{h\sum_{j=1}^{n}|u_j^{\text{exact}} - u_j^{\text{numerical}}|^2}, \quad L_{\max} = \max|u_j^{\text{exact}} - u_j^{\text{numerical}}|,$$

$$\text{Global Relative Error (GRE)} = \frac{\sum_{j=1}^{n}|u_j^{\text{exact}} - u_j^{\text{numerical}}|}{\sum_{j=1}^{n}|u_j^{\text{exact}}|}, \text{and ROC} = \frac{\log(\varepsilon^n/\varepsilon^{n+1})}{\log\left(\frac{n+1}{n}\right)}.$$

We begin with the following example.

Example 6.1. First, we consider the TFT Equation (2.1) with $\lambda_1 = \lambda_2 = 1$ and $\lambda_3 = \pi$ together with the exact solution $v(\xi,\tau) = \tau^3\sin^2\xi$. The analogous source function is specified by

$$f(\xi,\tau) = \left(\frac{6\tau^{3-\alpha}}{\Gamma(4-\alpha)} + \frac{6\tau^{4-\alpha}}{\Gamma(5-\alpha)} - (2\pi-1)\tau^3\right)\sin^2\xi - 2\pi\tau^3\cos^2\xi\,. \tag{6.1}$$

We select the tension parameter $\varsigma = 1.25$ for this example. Table 2 demonstrates the difference between the projected and existing methods in a period of RMS errors together with convergence order with $\varsigma = 1.25$, $\Delta\tau = 0.001$ at $\tau = 1$ for

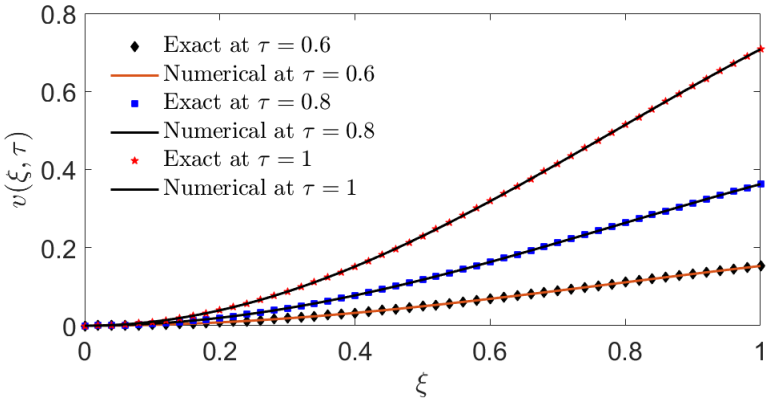

FIGURE 1. The exact and numerical $v(\xi, \tau)$ values with ς =1.25, α =1.5, M =30, $\Delta\tau$ =0.01 atτ =0.6, 0.8, and 1 for Example 6.1.

fractional orders α =1.75 and 1.95. Remarkably, the obtained results are better than those accomplished by CTBS and Sinc-Legender (degree 3) collocation methods [28, 41]. Tables 3 and 4 compare the projected and existing methods in terms of the L_2, L_∞ error norms with α =1.5, M =30 at τ =1 for various $\Delta\tau$, and with α =1.5, $\Delta\tau$ =0.001 at τ =1 for various M. It is very clear from these tables that the projected method results are better than those exhibited by the QBS Galerkin method as well as the CTBS collocation method [34, 41]. It is also followed that the convergence rate of the projected method is quadratic in the space variable and $2 - a$ order in the time variable. Figure 1 displays the comparison of the exact and numerical $v(\xi, \tau)$ with ς =1.25, α =1.5, M =30, $\Delta\tau$ =0.01 at τ =0.6, 0.8, and 1. A remarkable accord is recovered between exact and numerical solutions. Figure 2 shows the RMS error norms vs. space and fixed $\Delta\tau = 0.001$, as well as time grid sizes and fixed M =30 with α =1.2 and α =1.8. This figure shows that the RMS error norms are decreasing with increasing grid sizes. Figures 3 and 4 display the 3D exact and numerical $v(\xi, \tau)$, and absolute errors profile with ς =1.25, α =1.5, M =10, $\Delta\tau$ =0.02, and ς =1.25, α =1.5, M =30, $\Delta\tau$ =0.1 for $\tau \in [0, 1]$.

TABLE 2. The RMS error and ROC of the projected and existing methods for various M values with $\varsigma = 1.25$, $\Delta\tau = 0.001$ at $\tau = 1$, for Example 6.1.

M	$\alpha = 1.75$					$\alpha = 1.95$				
	Projected method	CTBS [41]	Sinc-L [28]	ROC	CPU time	Projected method	CTBS [41]	Sinc-L [28]	ROC	CPU time
5	2.05e-4	2.86e-4	9.94e-4	–	3.29	1.98e-4	2.81e-4	9.58e-4	–	3.30
10	3.50e-5	7.85e-5	1.60e-4	2.55	5.67	3.64e-5	7.50e-5	1.54e-4	2.44	5.56
15	1.06e-5	3.66e-5	3.71e-5	2.96	8.08	1.26e-5	3.55e-5	3.57e-5	2.62	8.09
20	3.82e-6	2.17e-5	1.05e-5	3.54	10.6	5.55e-6	2.15e-5	1.01e-5	2.84	10.4

Example 6.2. Next, we study the TFT Eq. (2.1) with $\lambda_1 = \lambda_2 = \lambda_3$ =1 in [0,1] together with the exact solution $v(\xi, \tau) = \left(\xi^2 - \xi\right)\tau$. The analogous source function is specified by

$$f(\xi, \tau) = \left(\frac{1}{\Gamma(3-\alpha)}\tau^{2-\alpha} + \tau\right)\left(\xi^2 - \xi\right) - 2\tau,$$

We fix the tension parameter ς =0.015 for this example. Table 5 demonstrates the assessment of projected and existing methods in a period of absolute errors with α =1.95, $\Delta\tau$ =0.01 at τ =1 for M =10. This table shows that the obtained results are better than those attained by CTBS and Sinc-Legender (degree 3) collocation methods [28, 41]. Table 6

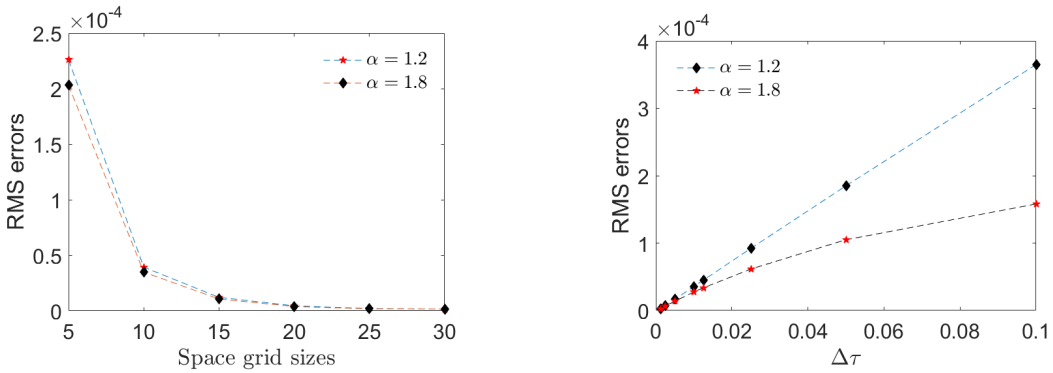

FIGURE 2. The RMS error norms vs. space grid size (left) and time grid size (right) for Example 6.1.

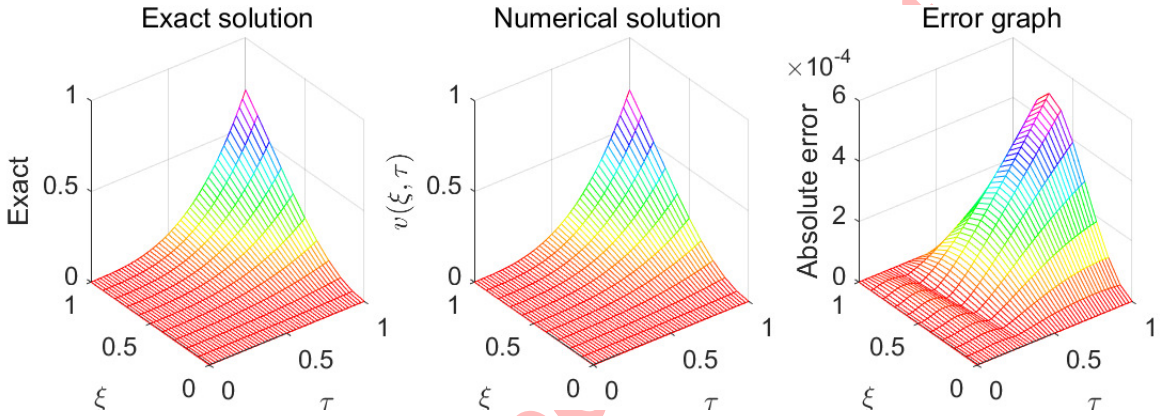

FIGURE 3. The 3D exact and numerical $\nu(\xi,\tau)$, and absolute error profile with $\varsigma = 1.25$, $\alpha = 1.5$, $M = 10$, $\Delta\tau = 0.02$, and $\tau \in [0,1]$ for Example 6.1.

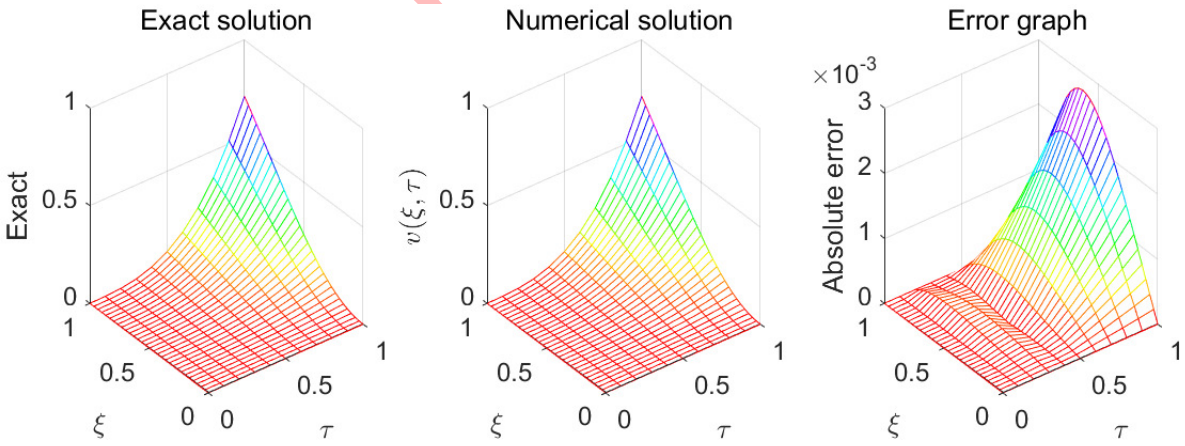

FIGURE 4. The 3D exact numerical $\nu(\xi,\tau)$ and absolute error profile with $\varsigma = 1.25$, $\alpha = 1.5$, for $M = 30$, $\Delta\tau = 0.1$, and $\tau \in [0,1]$ for Example 6.1.

TABLE 3. The comparison of methods with $\varsigma = 1.25$, $\alpha = 1.5$, $M = 30$ at $\tau = 1$ at various $\Delta\tau$, for Example 6.1.

$\Delta\tau$	L_2 Error			ROC	L_∞ Error			ROC	CPU
	Projected	QBS [34]	CTBS [41]		Projected	QBS [34]	CTBS [41]		time
0.1	1.900e-3	8.338e-3	2.830e-3	–	2.700e-3	1.297e-2	4.078e-3	–	0.18
0.05	1.000e-3	4.188e-3	1.369e-3	0.93	1.500e-3	6.501e-3	1.969e-3	0.85	0.27
0.01	2.159e-4	7.816e-4	2.631e-4	0.95	3.112e-4	1.216e-3	3.767e-4	0.98	0.97
0.005	1.035e-4	3.479e-4	1.332e-4	1.06	1.514e-4	5.454e-4	1.899e-4	1.04	2.03
0.001	1.186e-5	2.003e-5	3.271e-5	1.37	2.053e-5	3.397e-5	4.544e-5	1.24	15.5

TABLE 4. The comparison of the projected and existing methods with $\varsigma = 1.25$, $\alpha = 1.5$, $\Delta\tau = 0.001$ at $\tau = 1$ at various grid sizes, for Example 6.1.

M	L_2 Error			ROC	L_∞ Error			ROC	CPU time
	Projected	QBS [34]	CTBS [41]		Projected	QBS [34]	CTBS [41]		
5	5.754e-04	3.798e-03	3.280e-04	–	8.393e-04	4.929e-03	5.238e-04	–	3.29
10	1.275e-04	8.222e-04	1.101e-04	2.17	1.886e-04	1.096e-03	1.151e-04	2.15	5.90
15	4.547e-05	3.043e-04	5.840e-05	2.54	7.179e-05	4.080e-04	8.326e-05	2.38	8.11
20	1.855e-05	1.302e-04	4.331e-05	3.11	3.101e-05	1.717e-04	6.58e-05	2.91	10.49
25	1.619e-05	5.307e-05	3.641e-05	2.46	1.619e-05	7.052e-05	5.063e-05	2.91	13.54

illustrates RMS and L_∞ errors with M =30, for $\Delta\tau = 0.05$, 0.025, 0.02, 0.0125, and 0.01, and fractional orders α =1.4 and 1.95 at τ =1. This table confirms that error norms are very small and decrease with increasing temporal size. The 2D graph of exact and numerical $v(\xi,\tau)$ with α =1.95, M =15, $\Delta\tau$ =0.001 at τ =0.5, 0.75, and 1 are shown in Figure 5. Figure 6(a) indicates the 2D profile of the absolute errors with M =30, $\Delta\tau$ =0.001 at τ =1 for fractional order α =1.5, 1.75, and 1.95, while Figure 6(b) illustrates RMS, L_2, and L_∞ errors with α =1.95 and $\Delta\tau$ =0.005 for various grid sizes at τ =1. It can be viewed from Figures 6(a) and 6(b) that these errors are in order ($\approx 10^{-4}$). Figure 7(a) exhibits the 3D profile of exact and numerical $v(\xi,\tau)$, together with absolute errors of α =1.95, M =10, and $\Delta\tau$ =0.025 for $\tau \in [0,1]$, while Figure 7(b) describes it with α =1.95, M =40, and $\Delta\tau$ =0.01 for $\tau \in [0,1]$. A remarkable accord is recovered between exact and numerical solutions.

TABLE 5. The assessment of projected and existing methods in the period of absolute error with $\alpha = 1.95$, $\Delta\tau = 0.01$ at $\tau = 1$ for Example 6.2.

ξ	$M = 10$			
	Projected method	CPU time	CTBS [41]	Sinc-Legendre [28]
0.0	0	0.419	0	0
0.1	2.087e-05	0.409	1.52e-04	2.906e-04
0.2	4.275e-05	0.399	2.66e-04	3.789e-04
0.3	6.351e-05	0.406	3.45e-04	3.816e-04
0.4	7.843e-05	0.415	3.91e-04	3.641e-04
0.5	8.378e-05	0.405	4.06e-04	3.547e-04
0.6	7.843e-05	0.392	3.91e-04	3.641e-04
0.7	6.351e-05	0.397	3.45e-04	3.816e-04
0.8	4.275e-05	0.400	2.66e-04	3.789e-04
0.9	2.087e-05	0.406	1.52e-04	2.906e-04
1.0	0	0.395	–	0

TABLE 6. The error norms of the projected method with $\varsigma = 0.015$, $M = 30$, and various $\Delta\tau$ at $\tau = 1$ for Example 6.2.

$\Delta\tau$	$\alpha = 1.4$			CPU (s)	$\alpha = 1.95$			CPU (s)
	RMS	L_2	L_∞		RMS	L_2	L_∞	
0.05	1.19e-04	6.72e-04	9.46e-04	0.383	1.55e-04	8.77e-04	1.20e-03	0.400
0.025	5.20e-05	2.95e-04	4.14e-04	0.639	7.09e-05	4.01e-04	5.65e-04	0.603
0.02	3.96e-05	2.24e-04	3.15e-04	0.707	5.22e-05	2.95e-04	4.16e-04	0.721
0.0125	2.18e-05	1.23e-04	1.73e-04	1.115	2.24e-05	1.27e-04	1.80e-04	1.044
0.01	1.62e-05	9.17e-05	1.29e-04	1.343	1.19e-05	6.72e-05	9.64e-05	1.291

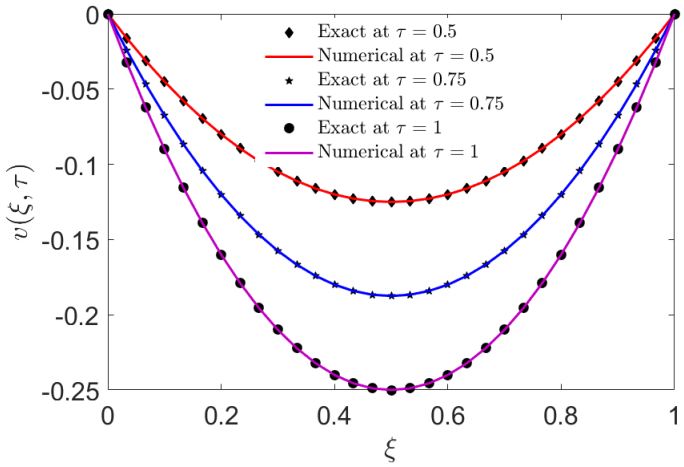

FIGURE 5. The exact and numerical $v(\xi, \tau)$ with α =1.95, M =15, $\Delta\tau$ =0.001 at τ =0.5, 0.75, and 1 for Example 6.2.

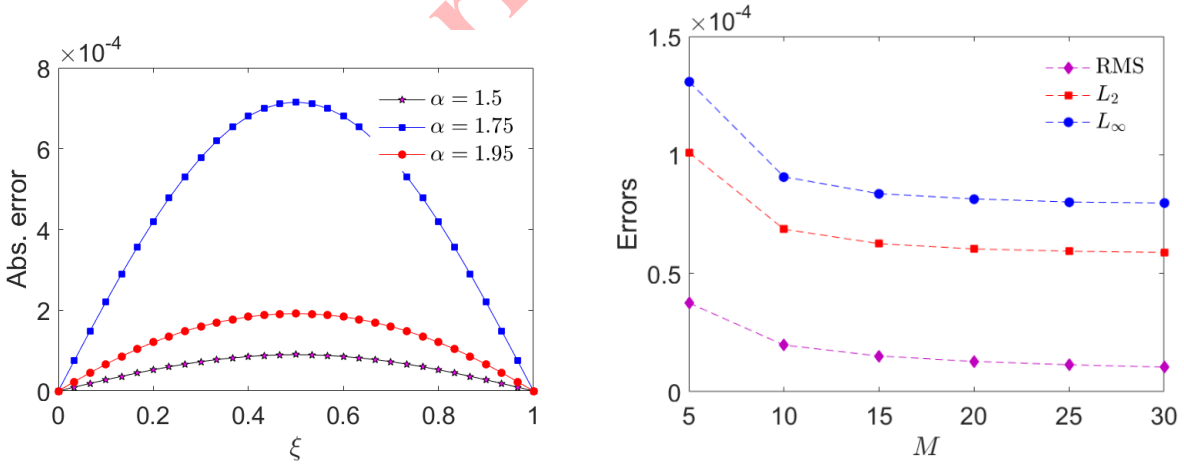

(a) (b)

FIGURE 6. The 2D errors graph for Example 6.2 with (a) M =30, $\Delta\tau$ =0, and α =1.5, 1.75, and 1.95 (b) α =1.95 and $\Delta\tau$ =0.005 at τ =1 for Example 6.2.

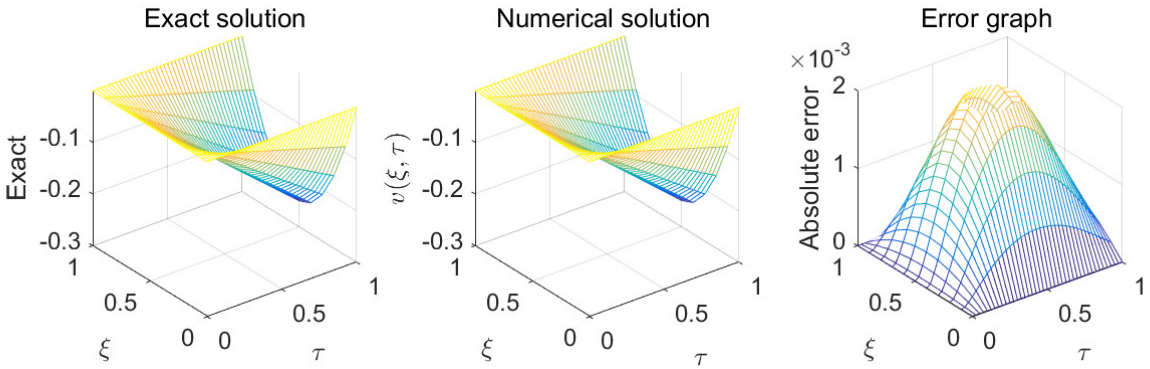

(a) $M = 10$, $\Delta\tau = 0.025$.

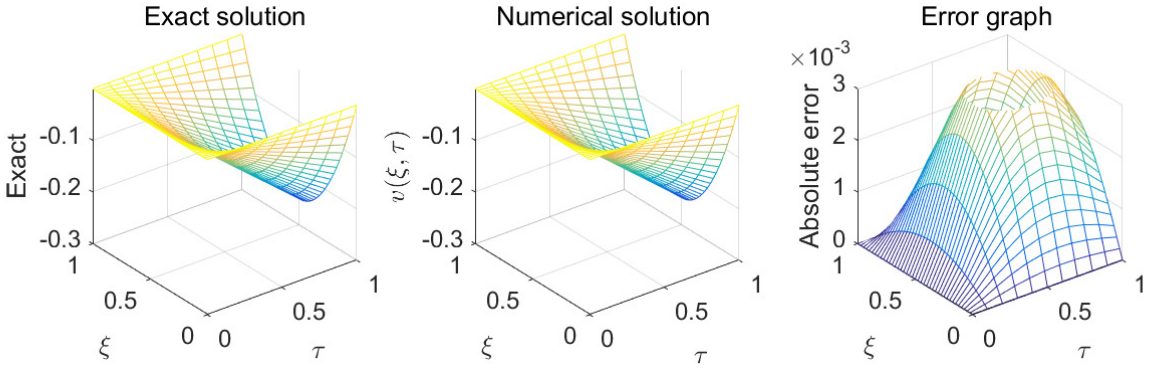

(b) $M = 40$, $\Delta\tau = 0.01$.

FIGURE 7. The 3D profile of exact numerical $v(x,t)$ and absolute error for $\alpha = 1.95$, $\tau \in [0,1]$, with (a) $M = 10$, $\Delta\tau = 0.025$ and (b) $M = 40$, $\Delta\tau = 0.01$ (Example 6.2).

Example 6.3. Now, we consider the TFT Eq. (2.1) with $\lambda_1 = \lambda_2 = \lambda_3 = 1$ in [0,1] together with the exact solution $v(\xi,\tau) = \tau^\alpha \tan\xi$. The analogous source function is specified by $f(\xi,\tau) = \alpha(1+\tau)\tan\xi\,\Gamma(\alpha) - 2\tau^\alpha \tan^3\xi - \tau^\alpha \tan\xi$. We fix the tension parameter $\varsigma = 0.15$ for this example. Table 7 compares the projected and the CTBS method [41] in terms of RMS and L_2 errors with tension parameter $\varsigma = 0.15$ and fractional order $\alpha = 1.5$ for $\Delta\tau = 0.01$ and various M at $\tau = 1$, while Table 8 exhibits it for $M = 40$ with various values of $\Delta\tau$. These tables show that the obtained results are much better than ref. [41]. Table 9 demonstrates the RMS, L_2, and L_∞ errors of the projected method with $\varsigma = 0.15$, $\Delta\tau = 0.001$ at $\tau = 1$ for fractional orders $\alpha = 1.6$ and 1.8, and various grid sizes. One can see that error norms are decreasing on increasing grid sizes increase. Figure 8 displays the absolute error with $\varsigma = 0.15$, $\alpha = 1.5$, $M = 40$ at $\tau = 1$ for $\Delta\tau = 0.01$, 0.005, 0.0025, and 0.00125, whereas Figure 9 exhibits the 3D appearance of exact and numerical $v(\xi,\tau)$, and abs. errors for fractional orders $\alpha = 1.5$, 1.75, and 1.95 with $\varsigma = 0.15$, $M = 20$, $\Delta\tau = 0.002$, and $\tau \in [0,1]$. It can be viewed from Figures 8 and 9 that the abs. errors are in order ($\approx 10^{-3}$).

7. Conclusion

This work proposes a new collocation structure based on CUETTB-spline functions to approximate the Caputo TFT equation. This scheme is used for discretizing spatial derivatives, while the time-fractional derivative is discretized by Caputo's definition. The three examples have been considered to justify the accuracy and competence of the established method. It has been stated that the projected method provides superior results than those in [20, 34, 37, 41]. The

TABLE 7. Comparison of the projected and CTBS methods with $\varsigma = 0.15$, $\alpha = 1.5$, $\Delta\tau = 0.01$ for various M at $\tau = 1$ for Example 6.3.

M	RMS		L_2		CPU time
	Projected Method	CTBS [41]	Projected Method	CTBS [41]	
20	2.9695e-04	2.0100e-03	1.4000e-03	2.0593e-03	1.026
40	1.6599e-04	1.6212e-03	1.1000e-03	1.6414e-03	1.813
80	1.1017e-04	1.5285e-03	9.9771e-04	1.5381e-03	3.330
160	7.6854e-05	1.5076e-03	9.7821e-04	1.5123e-03	7.241

TABLE 8. Comparison of the projected and CTBS methods with $\varsigma = 0.15$, $\alpha = 1.5$ for $M = 40$ and various $\Delta\tau$ at $\tau = 1$ for Example 6.3.

Δt	RMS		L_2		CPU time
	Projected method	CTBS [41]	Projected method	CTBS [41]	
0.0125	2.0391e-04	1.8119e-03	1.3000e-03	1.8344e-03	1.414
0.0100	1.6599e-04	1.6212e-03	1.1000e-03	1.6414e-03	1.783
0.00125	3.4666e-05	6.4542e-04	2.2472e-04	6.5344e-04	20.538
0.0010	3.1001e-05	1.5285e-03	2.0102e-04	1.5285e-03	28.635

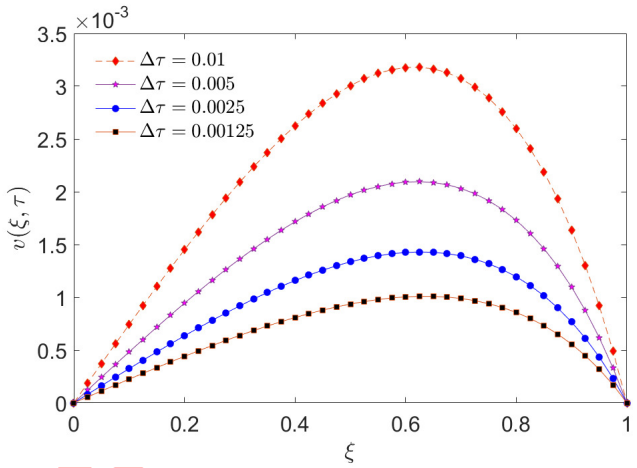

FIGURE 8. The absolute error with ς =0.15, α =1.5, M =40 at τ=1 for different $\Delta\tau$ for Example 6.3.

TABLE 9. The error norms of the projected method with $\varsigma = 0.15$, $\Delta t = 0.001$ at $\tau = 1$ for Example 6.3.

M	$\alpha = 1.6$			$\alpha = 1.8$			CPU time
	RMS	L_2	L_∞	RMS	L_2	L_∞	
10	6.272e-04	2.200e-03	3.200e-03	5.356e-04	1.900e-03	2.800e-03	8.009
15	2.631e-04	1.100e-03	1.600e-03	2.102e-04	8.682e-04	1.300e-03	11.609
20	1.514e-04	7.110e-04	1.000e-03	1.121e-04	5.266e-04	7.975e-04	14.690
25	1.036e-04	5.386e-04	7.726e-04	7.111e-05	3.698e-04	5.571e-04	18.248
30	7.871e-05	4.455e-04	6.364e-04	5.036e-05	2.850e-04	4.290e-04	21.685
35	6.402e-05	3.896e-04	5.547e-04	3.846e-05	2.340e-04	3.518e-04	25.179
40	5.451e-05	3.534e-04	5.020e-04	3.101e-05	2.010e-04	3.019e-04	31.320

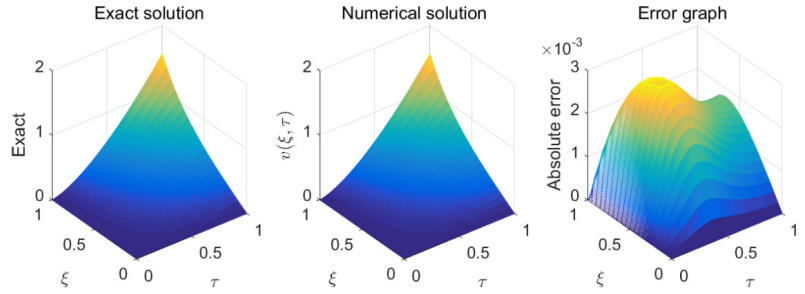

(a) First case.

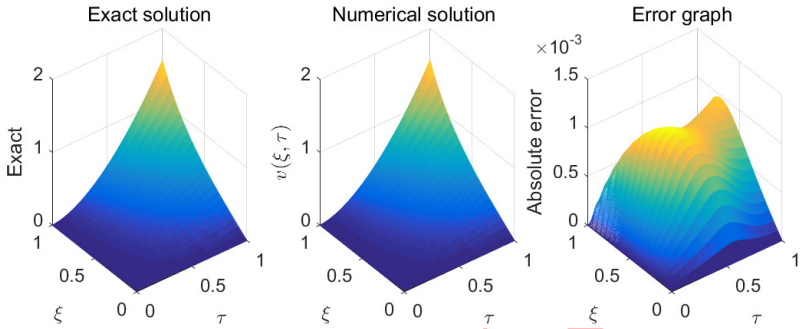

(b) Second case.

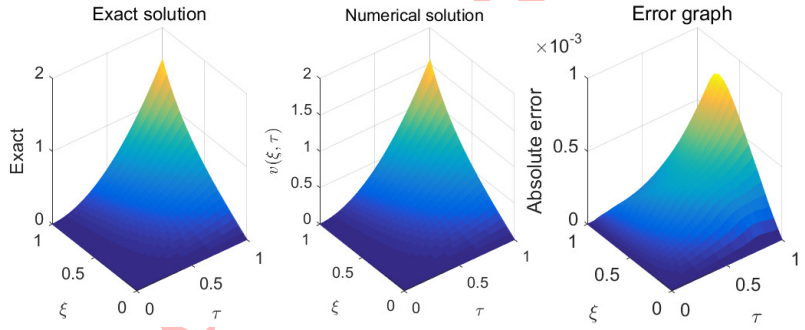

(c) Third case.

FIGURE 9. The 3D profile of exact numerical $\mathcal{V}(\xi,\tau)$ and absolute error with $\alpha = 1.95$, $\tau \in [0,1]$.

graphical outcomes are also displayed, which validate the accuracy of the proposed scheme. As we can see, Figures 1 and 5 are clear representations of the smoothness between numerical and exact solutions, while Figures 2, 3, 6–9 show that absolute and RMS errors are very low ($\approx 10^{-3}$ to 10^{-4}). It is established that the projected method is unconditionally stable for the discretized system of the TFT equation. It is also found that the convergence of the projected method is of $O(h^2, \tau^{2-\alpha})$. The numerical analysis proves that the projected method is straightforward and yields very accurate results.

FUNDING

Not available.

Availability of data and materials

Not applicable.

Declarations:

The authors declare that they have no competing interests.

Competing interests

All the authors declare no conflict of interest

Authors' contributions

The author has read and confirmed the final manuscript and participated equally in the manuscript.

Acknowldegmnt

The authors would like to thank the anonymous reviewers and editor for providing helpful comments and suggestions, which further improved the quality of the manuscript.

References

[1] O. F. Azhar, F. Naeem, F. Mofarreh, and J. Kaflem, *Numerical analysis of the fractional-order telegraph equations*, J. Func. Spac., *2021* (2021), 1–14.
[2] Z. Abdollahy, Y. Mahmoudi, A. Salimi Shamloo, and M. Baghmisheh, *Haar Wavelets method for time fractional Riesz space telegraph equation with separable solution*, Rep. Math. Phys., *89*(1) (2022), 81–96.
[3] M. Asgari, R. Ezzati, and T. Allahviranloo, *Numerical solution of time-fractional order telegraph equation by Bernstein polynomials operational matrices*, Math. Probl. Eng., *2016* (2016), 1–6.
[4] M. Amin, M. Abbas, D. Baleanu, M. K. Iqbal, and M. B. Riaz, *Redefined Extended Cubic B-Spline Functions for Numerical Solution of Time-Fractional Telegraph Equation*, Comput. Model. Eng. Sci., *127*(1) (2021), 361–384.
[5] N. Alinia and M. Zarebnia, *Trigonometric tension B-spline method for the solution of problems in calculus of variations*, Comput. Math. and Math. Phys., *58* (2018), 631–641.
[6] J. Banasiak and J. R. Mika, *Singularly perturbed telegraph equations with applications in the random walk theory*, J. Appl. Math. Stoch. Anal., *11*(1) (1998), 9–28.
[7] H. Bansu and S. Kumar, *Numerical Solution of Space and Time Fractional Telegraph Equation: A Meshless Approach*, Int. J. Nonlinear Sci. Numer. Simul., *20*(3-4) (2019), 325–337.
[8] S. Das, K. Vishal, P. K. Gupta, and A. Yildirim, *An approximate analytical solution of time-fractional telegraph equation*, Appl. Math. Comput., *217*(18) (2011), 7405–7411.
[9] H. Eltayeb, Y. T. Abdalla, I. Bachar, and M. H. Khabir, *Fractional telegraph equation and its solution by natural transform decomposition method*, Symmetry, *11* (2019), 334.
[10] W. Hachbusch, Integral equations theory and numerical treatments, Birkhäuser Basel, 1995.
[11] V. R. Hosseini, W. Chen, and Z. Avazzadeh, *Numerical solution of fractional telegraph equation by using radial basis functions*, Engineering Analysis with Boundary Elements, *38* (2014), 31–39.
[12] M. H. Heydari, M. R. Hooshmandasl, and F. Mohammadi, *Two-dimensional Legendre wavelets for solving time-fractional telegraph equation*, Adv. Appl. Math. Mech., *6*(2) (2014), 247–260.
[13] G. Hariharan, R. Rajaraman, and M. Mahalakshmi, *Wavelet method for a class of space and time fractional telegraph equations*, Int. J. Phys. Sci., *7* (2012), 1591–1598.
[14] M. S. Hashmi, U. Aslam, J. Singh, and K. S. Nisar, *An efficient numerical scheme for fractional model of telegraph equation* , Alex. Eng. J., *61*(8) (2022), 6383–6393.
[15] M. S. Hashemi and D. Baleanu,*Numerical approximation of higher-order time-fractional telegraph equation by using a combination of a geometric approach and method of line*, J. Comput. Phys., *316* (2016), 10–20.
[16] W. Ibrahim and L. K. Bijiga, *Neural network method for solving time-fractional telegraph equation*, Math. Probl. Eng., *2021* (2021), 1–10.

[17] P. Jordan and A. Puri, *Digital signal propagation in dispersive media*, J. Appl. Phys., *85*(3) (1999), 1273–1282.
[18] A. A. Kilbas, H. M. Srivastava, J. J. Trujillo, *Theory and applications of fractional differential equations*, Elsevier Science BV, Amsterdam, 2006.
[19] K. Kumar, R. K. Pandey, and S. Yadav, *Finite difference scheme for a fractional telegraph equation with generalized fractional derivative terms*, Stat. A Mech. Appl., *535* (2019), 122271.
[20] S. Momani, *Analytic and approximate solutions of the space- and time-fractional telegraph equations*, Appl. Math. Comput., *176* (2005), 1126–1134.
[21] A. K. Mishra, S. Kumar, and A. K. Shukla, *Numerical approximation of fractional telegraph equation via Legendre collocation technique*, Int. J. Appl. Comput. Math., *7* (2021), 198.
[22] N. Mollahasani, M. M. M. Moghadam, and K. Afrooz, *A new treatment based on hybrid functions to the solution of telegraph equations of fractional order*, Appl. Math. Model., *40*(4) (2016), 2804–2814.
[23] E. Orsingher and L. Beghin, *Time-fractional telegraph equations and telegraph processes with brownian time*, Probab. Theory Relat. Fields, *128* (2004), 141–160.
[24] E. Orsingher and X. Zhao, *The space-fractional telegraph equation and the related fractional telegraph process*, Chin. Ann. Math. B, *24*(1) (2003), 45–56.
[25] I. Podlubny, *Fractional differential equations* , Academic Press, 1999.
[26] P. Rahimkhani, O. Yadollah, and S. Sabermahani, Bernoulli wavelet least squares support vector regression: Robust numerical method for systems of fractional differential equations, Math. Meth. Appl. Sci., *46*(17) (2023), 17641–17659.
[27] P. Roul, *A high accuracy numerical method and its convergence for time-fractional Black-Scholes equation governing European options*, Appl. Numer. Math., *151* (2020), 472–493.
[28] N. H. Sweilam, A. M. Nagy, and A. A. El-Sayed, *Solving Time-Fractional Order Telegraph Equation Via Sinc-Legendre Collocation Method*, Mediterr. J. Math., *13* (2016), 5119–5133.
[29] N. H. Sweilam, A. M. Nagy, and A. A. El-Sayed, *Sinc-Chebyshev collocation method for time-fractional order telegraph equation*, Appl. Comput. Math., *19*(2) (2020), 162–174.
[30] F. A. Shah, M. Irfan, K. S. Nisar, and R. T. Matoog, *Fibonacci wavelet method for solving time-fractional telegraph equations with Dirichlet boundary conditions*, Results Phys., *24* (2021), 104123.
[31] S. Sabermahani, Y. Ordokhani, and S. A. Yousefi, *Numerical approach based on fractional-order Lagrange polynomials for solving a class of fractional differential equations*, Comp. Appl. Math., *37* (2018), 3846–3868.
[32] S. Sabermahani, Y. Ordokhani, and S. A. Yousefi, *Two-dimensional Müntz–Legendre hybrid functions: theory and applications for solving fractional-order partial differential equations*, Comp. Appl. Math., *39* (2020), 111.
[33] J. C. Strikwerda, Finite difference schemes and partial differential equations, 2nd edition, SIAM, 2004.
[34] O. Tasbozan and A. Esen, *Quadratic B-spline Galerkin method for numerical solutions of fractional telegraph equations*, Bull. Math. Sci. Appl., *18* (2017), 23–39.
[35] O. Tasbozan and A. Esen, *Collocation solutions for the time fractional telegraph equation using cubic B-spline finite elements*, An. Univ. Vest Timiş. Ser. Mat.-Inf., *57*(2) (2019), 131–144.
[36] V. A. Vyawahare and P. Nataraja, *Fractional order modelling of neutron transport in a nuclear reactor*, Appl. Math. Model., *37*(23) (2013), 9747–9767.
[37] L. Wei, H. Dai, D. Zhang et al., *Fully discrete local discontinuous Galerkin method for solving the fractional telegraph equation*, Calcolo, *51* (2014), 175–192.
[38] G. Wang and M. Fang, *Unified and extended form of three types of splines*, J. Comput. Appl. Math., *216* (2008), 498–508.
[39] Y. L. Wang, M. J. Du, C. L. Temuer, and D. Tian, *Using reproducing kernel for solving a class of time fractional telegraph equation with initial value conditions*, Int. J. Comput. Math., *95* (2018), 1609–1621.
[40] X. Xu and D. Xu, *Legendre wavelets direct method for the numerical solution of time-fractional order telegraph equations*, Mediterr. J. Math., *15* (2018), 27.
[41] M. Yaseen and M. Abbas, *An efficient cubic trigonometric B-spline collocation scheme for the time-fractional telegraph equation*, Appl. Math. J. Chin. Univ., *35* (2020), 359–378.